



Enhanced electrochemical performance of Mg₂Ni alloy prepared by rapid quenching in magnetic field



Chenxi Jiang^a, Haiyan Wang^{a,*}, Yazhi Wang^a, Xiangrong Chen^a, Yougen Tang^{a,*},
Zuming Liu^b, Hualin Xie^c

^a Key Laboratory of Resources Chemistry of Nonferrous Metals, Ministry of Education, School of Chemistry and Chemical Engineering, Central South University, Changsha 410083, PR China

^b State Key Laboratory for Powder Metallurgy, Central South University, Changsha 410083, PR China

^c School of Chemistry and Chemical Engineering, Yangtze Normal University, Fuling 408100, PR China

HIGHLIGHTS

- Mg₂Ni alloy was rapidly quenched in a static magnetic field.
- The as-prepared alloy has directional columnar structures and high internal strain.
- High quenching rate goes against the formation of directional columnar crystals.
- The as-prepared alloy exhibits improved electrochemical performance.

ARTICLE INFO

Article history:

Received 31 October 2012

Received in revised form

13 March 2013

Accepted 15 March 2013

Available online 26 March 2013

Keywords:

Hydrogen storage alloy

Rapid quenching

Magnetic field

Electrochemical performance

ABSTRACT

Mg₂Ni alloy prepared by vacuum induction melting is rapidly quenched in the presence of an external magnetic field. The effects of magnetic field on the microstructure and electrochemical hydrogen storage behavior of Mg₂Ni alloy are well investigated for the first time. X-ray diffraction (XRD), scanning electron microscope (SEM) and energy dispersive spectroscopy (EDS) studies show that the applied magnetic field results in a preferred orientation growth during the rapid solidification of alloy melt, which induces the generation of columnar crystals. Meanwhile, decreased grain size and increased internal strain are noted for this alloy, as well as the eliminated composition segregation. It is found on the charge–discharge experiments that the as-prepared alloy displays an increased capacity and improved cycle stability compared to the alloys without magnetic field treatment. The potentiodynamic polarization results indicate that the Mg₂Ni alloy exhibits relatively high corrosion resistance against the alkaline solution. Electrochemical impedance spectroscopy (EIS) and cyclic voltammetry (CV) results demonstrate enhanced electrochemical kinetics for the treated Mg₂Ni alloy, consistent with the enhanced electrochemical properties.

© 2013 Elsevier B.V. All rights reserved.

1. Introduction

Hydrogen is considered to play significant roles in the future automotive applications. However, the effective storage of hydrogen is the bottleneck of its practical application. Among various materials, hydrogen storage alloys have been widely used as the negative electrode materials for nickel metal hydride batteries, which are generally regarded as the preferred power sources for portable power tools, hybrid electric vehicles (HEVs) and plug-

in hybrid electric vehicles (PHEVs) [1]. Since traditional AB₅-type hydrogen storage alloys are restricted for the low capacity and relatively high price, Mg-based alloys, particularly the Mg₂Ni-type alloys, appear to be promising materials due to their advantages of lightweight, low-cost and high hydrogen storage capacity. Note that Mg₂Ni-type alloys still suffer from poor cycling stability and inferior kinetics [2]. Accordingly, it is of great importance to develop novel strategies to address such issues.

Considerable studies have been done in order to improve the hydrogen storage properties of Mg₂Ni. Using high energy ball milling to prepare amorphous phase is a powerful way to enhance the electrochemical performance of hydrogen storage alloy [3,4], but the poor cycling stability due to the fact that the meta-stable

* Corresponding authors. Tel.: +86 0731 8830886; fax: +86 0731 8879616.

E-mail addresses: wanghy419@126.com (H. Wang), ygtang@csu.edu.cn (Y. Tang).

amorphous structures formed by ball milling tended to vanish sharply during absorbing/desorbing cycles [5], and the high energy consumption are insurmountable obstacles. Rapid quenching is also an effective method to ameliorate composition homogeneity, which is beneficial to improve the electrochemical cycling stability of AB₅-type alloys [6–8]. Unfortunately, the discharge capacity and the cycle life are always contradictory due to the decrease in the electrocatalytic activity and hydrogen diffusion rate caused by rapid solidification [9]. There are some reports on the preparation of Mg-based alloys by rapid quenching, in which it is found that the key factor to reach a high discharge capacity and long cycle life is to impede the crystallization of amorphous materials and prevent the corrosion of alloys in alkaline solution [10–12]. It is generally believed that the columnar crystals with a similar direction show a good resistance to corrosion during charging/discharging cycles [7] and supply channels for hydrogen diffusion [13], thus increase the discharge capacity and improve the cycle life.

Recently, magnetic field treatment in preparation of metallic materials has drawn increasing concerns. Investigations have suggested that magnetic field could change the equilibrium partition coefficient [14], refine the grain size [15], diminish the segregation ratio [16], and provide thermoelectromagnetic convection and magnetic damping [17]. In addition, it seems a feasible way to get specific structured materials using magnetic field to control the directional growth of crystal grains, whose driving force is related to the magnetocrystalline anisotropy energy [18–20].

In this work, a static magnetic field of 0.5 T was applied during the rapid solidification of Mg₂Ni alloy melt and its effects on the structure and electrochemical properties of the Mg₂Ni alloy were investigated for the first time. By taking the advantages of magnetic field treatment in combination with rapid quenching, the as-treated Mg₂Ni alloy exhibited much better electrochemical performance. Herein, quenching in the magnetic field could be considered as a very promising strategy for modification of Mg₂Ni alloy.

2. Experimental

2.1. Sample preparation

The starting raw alloy sample of Mg₂Ni was prepared by induction melting and casting from Mg and Ni blocks (purity above 99.9%). Positive pressure protection and repeated melting were employed to prevent massive Mg evaporation and ensure composition homogeneity in view of the low melting point and the high vapor pressure of Mg. The as-cast alloy was enveloped in a quartz tube with an inner diameter of 10 mm after being polished and broken into small pieces. Then it was re-melted and subsequently rapidly quenched with and without a magnetic field of 0.5 T. For convenience, the alloys rapidly quenched with and without magnetic field were denoted as MFRQ and RQ alloy in the following context, respectively. The apparatus is shown in Fig. 1. The cooling rate is expressed by the surface velocity of the copper roller as it is difficult to be measured accurately.

2.2. Sample characterization

Phase structures of the as-cast, RQ and MFRQ alloys were determined by a Bruker D8 Advance X-ray diffractometer with Cu K α radiation at 40 kV and 30 mA in the range from 10° to 80° with the scan speed of 4° min⁻¹. Ribbon sample for XRD analysis was prepared by putting several ribbon pieces together and embedding them into the denture base resin.

The microscopic structures were observed by a scanning electron microscope (Nova NanoSEM 230) linked with an energy dispersive spectrometer.

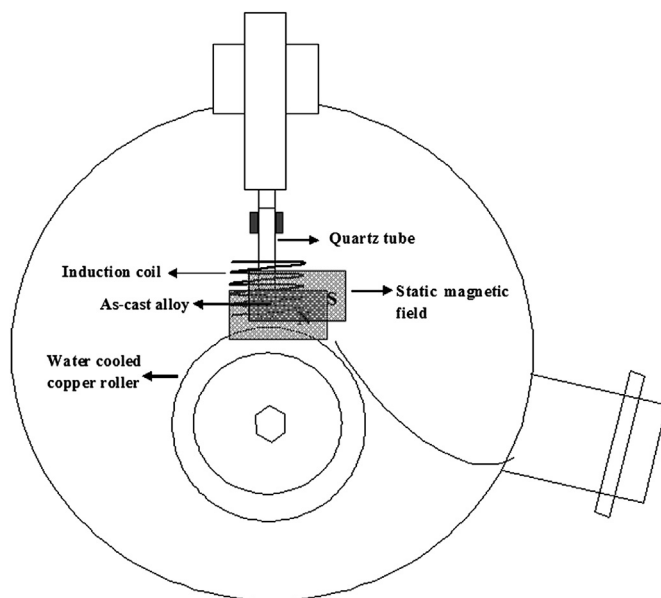


Fig. 1. Schematic illustration of the rapid quenching setup.

2.3. Electrochemical characterizations

All the samples were mechanically ground into powders of about 74 μ m in size. Then they were mixed with carbonyl nickel powder in a weight ratio of 1:3 (total mass of 0.4 g). The negative electrode was constructed by fixing the above mixture in a special mold and pressing into a round pellet of 10 mm in diameter. Electrochemical measurements were performed at 298 K in a standard open tri-electrode electrolysis cell, consisting of a hydrogen storage alloy electrode, a sintered Ni(OH)₂/NiOOH counter electrode and a Hg/HgO reference electrode immersed in 6 M KOH electrolyte. The discharge capacities and cycle life of the alloys were measured by galvanostatic method. Each electrode was charged at 20 mA g⁻¹ for 10 h followed by a rest of 10 min, and then discharged at 20 mA g⁻¹ to a cut-off potential of -0.6 V (vs. Hg/HgO).

Potentiodynamic polarization technique was employed to evaluate the corrosion resistance of the as-prepared alloys in alkaline solution at the scan rate of 0.1 mV s⁻¹ from -0.9 to -0.7 V (vs. Hg/HgO). EIS and CV experiments were measured to investigate the electrochemical kinetics of the alloys. All the above tests were carried out by a CHI660 electrochemical workstation system. EIS test was conducted at 50% depth of discharge.

Unless specially indicated, the cooling rate of the RQ and MFRQ alloys was fixed at 15 m s⁻¹.

3. Results and discussion

3.1. Morphological characterization

Fig. 2 shows the SEM images of the as-cast, RQ and MFRQ alloys. The results of EDS collected at different sections are listed in Table 1. It can be derived from Fig. 2(a) and (b) that the rapid quenching treatment not only alters the morphologies of Mg₂Ni alloy from a typical coarse dendrite structure to a refined flake-like structure, but also eliminates the secondary phase (denoted as A). According to the element content by EDS, A should be MgNi₂ phase and there is a higher content of Mg in the as-cast alloy. Fig. 2(c) and (d) shows the morphologies of the MFRQ alloy on the sections perpendicular (transverse) and parallel (longitudinal) to the magnetic field, respectively. Apparently, small equiaxed structures are formed on

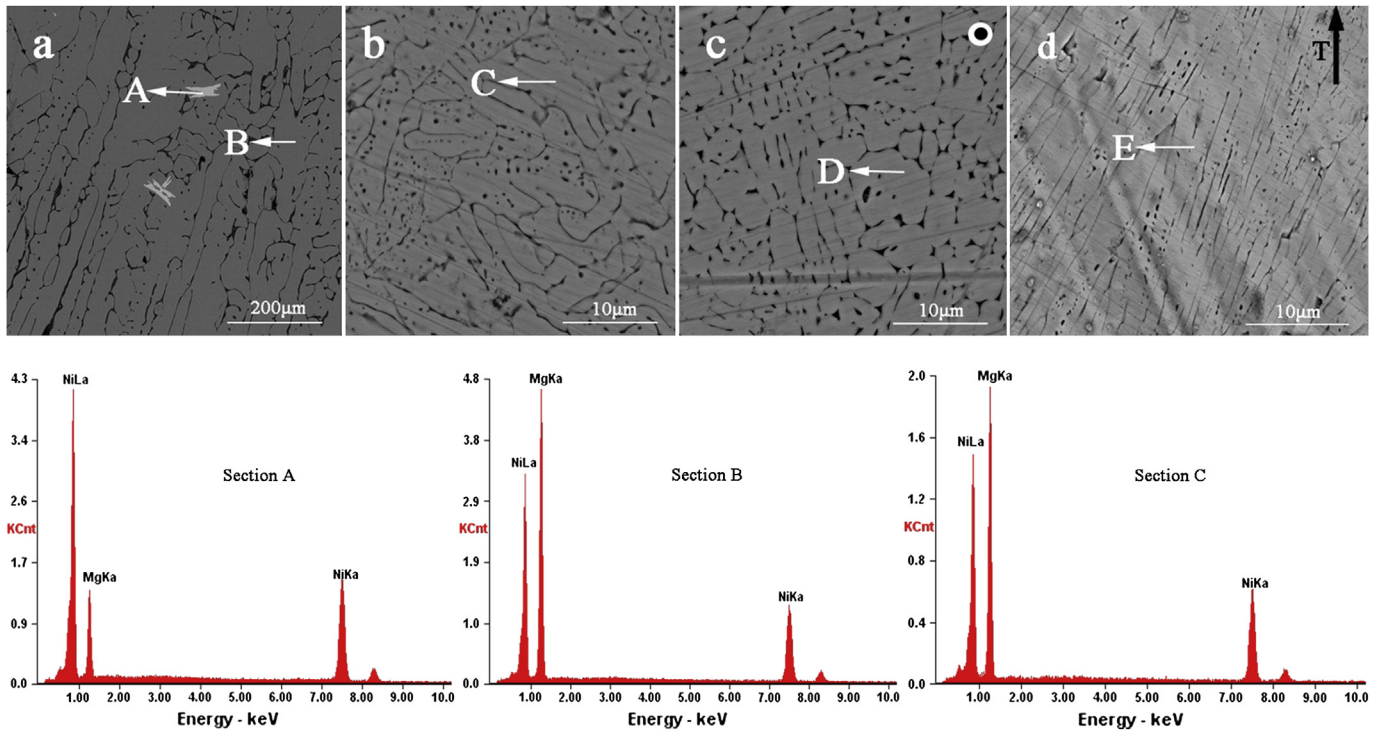


Fig. 2. SEM images of the ribbon samples and typical EDS spectra of section A, B and C: (a) as-cast alloy; (b) RQ alloy; (c) transverse section, MFRQ alloy; (d) longitudinal section, MFRQ alloy.

Table 1
Compositions of different sections measured by EDS.

Elements	Section A (at %)	Section B (at %)	Section C (at %)	Section D (at %)	Section E (at %)
Mg	37.13	71.20	67.75	68.31	68.06
Ni	62.87	28.80	32.25	31.69	31.94

the plane perpendicular to the magnetic field due to the influence of internally produced Lorentz force, which will restrain the flow of melting alloy and break up the dendrites. On the contrary, directional columnar structures are formed on the plane parallel to the magnetic field.

Fig. 3 displays the SEM images of the MFRQ alloys prepared at different quenching rates (5 and 30 m s⁻¹). Evidently, with the increase of quenching rate, the growth of grains tends to be more

random, indicating a negative effect on the formation of the directional columnar crystals. It could be explained as follows: when the surface velocity of copper roller is very fast, 30 m s⁻¹ for example, the interaction duration between the magnetic field and alloys is very short, therefore imposing very limited effect on the crystal growth. With this regard, the final crystal morphology is largely controlled by the cooling rate.

3.2. XRD phase analysis

The XRD patterns of the different samples are shown in Fig. 4. As seen, all three samples could be easily indexed into the Mg₂Ni phase on the basis of the standard PDF card (No. 35-1225). It should be noted that a trace amount of Mg is detected in the as-cast alloy, while not in RQ alloy and MFRQ alloy, indicating that the rapid quenching treatment could contribute to the crystal formation.

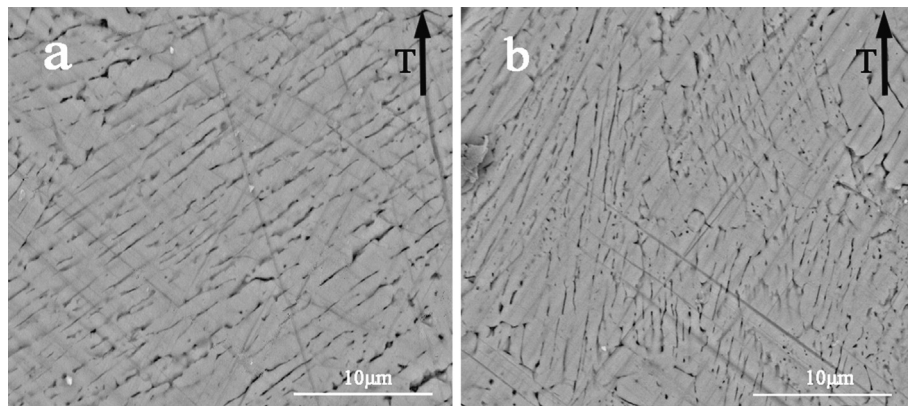


Fig. 3. SEM images of the MFRQ alloys prepared at quenching rate of 5 m s⁻¹ (a) and 30 m s⁻¹ (b).

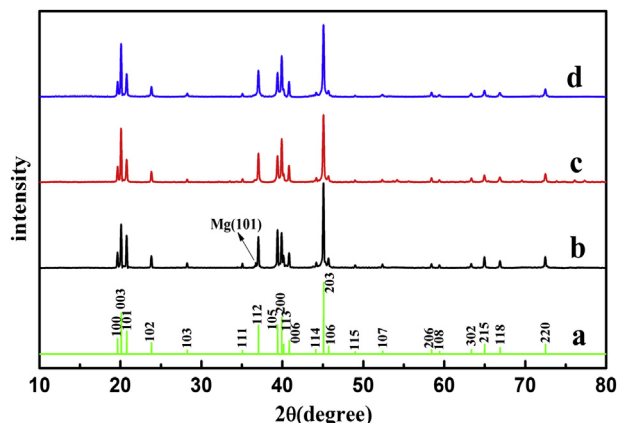


Fig. 4. XRD patterns of the as-prepared samples: (a) standard PDF card (No. 35-1225); (b) as-cast alloy; (c) RQ alloy; (d) MFRQ alloy.

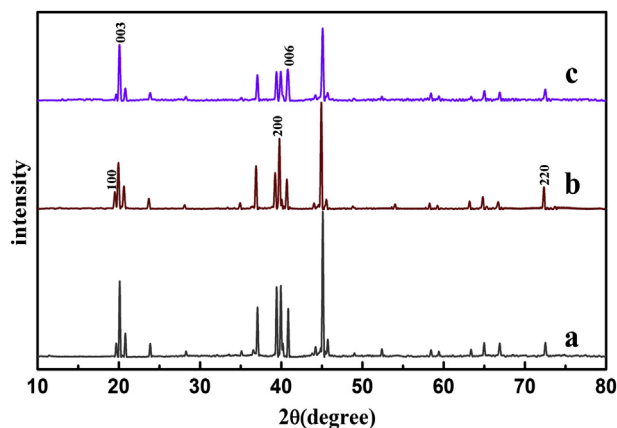


Fig. 5. XRD patterns of the ribbon samples: (a) RQ alloy; (b) longitudinal section, MFRQ alloy; (c) transverse section, MFRQ alloy.

Besides, no MgNi_2 phase is detectable probably because of their too low content. Results above demonstrate the high purity and good crystallinity of the RQ and MFRQ alloys.

The XRD profiles of the ribbon samples are presented in Fig. 5. On the section perpendicular to the magnetic field, the intensity of the (003) and (006) peaks increases in comparison with that of the RQ alloy; while on the section parallel to the magnetic field

direction, the intensity of the (100), (200) and (220) peaks is relatively enhanced. This confirms a remarkable magnetic anisotropy of the Mg_2Ni alloys, a driving force for preferred orientation growth [21]. Therefore, the formation of the directional columnar structures can be attributed to the magnetic force that renders the crystals of paramagnetic Mg_2Ni alloy grow along the easy magnetization axis direction.

Diffraction line broadening observed in XRD patterns can be ascribed to small crystallite dimensions and lattice imperfections [22]. When the grain size is above 100 nm, the broadening caused by the refinement of crystal grains can be negligible [23], making internal lattice strain the main factor. The micro-strain can be calculated according to the following equation [22]:

$$\varepsilon = \frac{\beta_n \cos \theta}{4 \sin \theta} \quad (1)$$

where ε is the value of the lattice strain and β_n is the line width. As shown in Fig. 6, the lattice strain is proportional to the slope of the straight line.

It is understandable that defects such as dislocations, stacking faults and grain boundaries are introduced during the rapid solidification of the alloy melt, yielding a fine grain size and increased internal strain. When the magnetic field was imposed, transmission of energy into the alloy from the magnetic field may occur, thus certain amount of internal energy would be stored and lead to non-stabilization of the lattice. As a consequence, a magnetic-field-induced strain [24] would be raised in the MFRQ alloy.

3.3. Charge–discharge properties

Fig. 7(A) shows the variation of the discharge capacities of different alloys vs. the number of cycles. The cycle stability of the alloy is symbolized by the capacity retention rate at the 15th cycle, defined as $S_{15} = C_{15}/C_{\max} \times 100\%$, where C_{\max} is the maximum discharge capacity and C_{15} is the discharge capacity at the 15th cycle. The MFRQ alloy delivers a maximum capacity of $142.05 \text{ mAh g}^{-1}$ with capacity retention ratio of 56.5% after 15 cycles. In contrast, the maximum capacity of the as-cast alloy is only 71.38 mAh g^{-1} and capacity retention ratio is 26.7%. Note that the discharge capacity of the as-cast alloy decays gradually with the cycle number, while the discharge capacity of the MFRQ alloy firstly increases from 89.02 mAh g^{-1} at the first cycle to the maximum at the 5th cycle, and then decreases gradually afterward. There is no doubt that the serious corrosion of Mg_2Ni in the alkaline solution directly leads to the decrease of discharge capacity and the activation process is easy to be covered. In contrast, the anti-corrosive columnar structures of the MFRQ alloy do alleviate the influence of corrosion on the capacity fade. Hence, the activation process of the MFRQ alloy is relatively more obvious.

The relationship of the potential and capacity in the 5th cycle is shown in Fig. 7(B). Generally, the small difference between charge and discharge voltage implies weak polarization for the electrode and obvious discharge plateau corresponds to high capacity. As can be seen, the MFRQ alloy owns the lowest charge voltage and an obvious discharge plateau ranging from 1.0 V to 0.9 V, while the as-cast and RQ alloys have relatively higher charge voltage and no apparent plateau, suggesting the strategy of rapid quenching and magnetic field treatment together is greatly beneficial for the electrochemical performance of Mg_2Ni alloy.

To study the effect of the directional columnar structures on the charge and discharge properties, evolution of the maximum discharge capacities and the cycle stabilities of different alloys with the quenching rate were investigated since the quenching rate influenced the crystal structure. In Fig. 8, among all the alloy

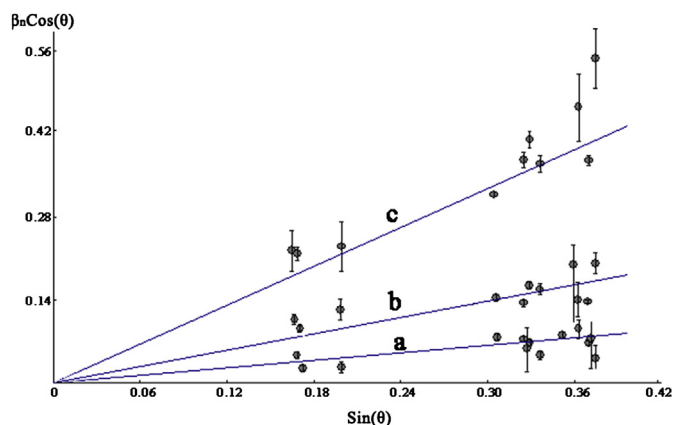


Fig. 6. Lattice strain plots: (a) as-cast alloy; (b) RQ alloy; (c) MFRQ alloy. (θ is the diffraction angle and β_n is the line width. Each point represents a diffraction peak).

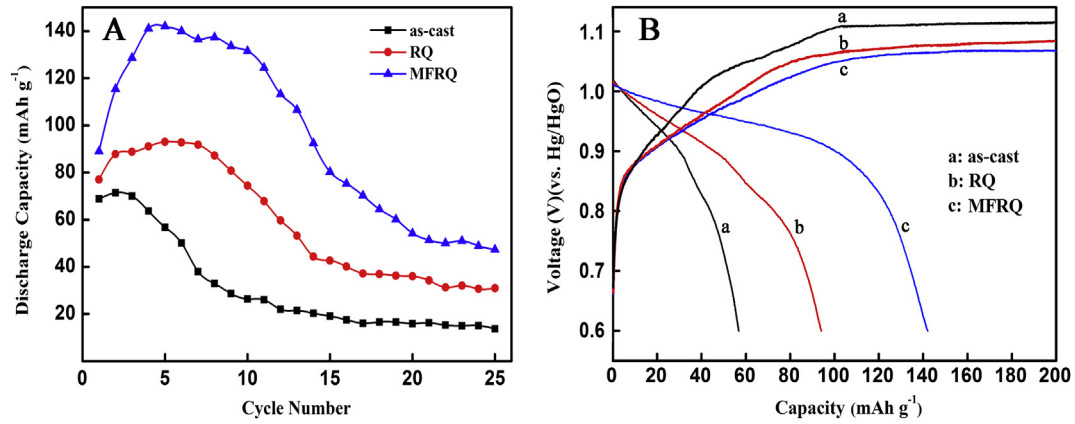


Fig. 7. Variation of the discharge capacities vs. the cycle number (A) and charge–discharge curves in the 5th cycle (B) for different alloys.

samples, the MFRQ alloy with the quenching rate of 15 m s^{-1} exhibits the highest discharge capacity and the best cycle stability. Zhang et al. [12] proved that high quenching rate was beneficial to the improvement of discharge capacity and cycle life, however, in our research, too much higher quenching rate gave a negative impact on the formation of the directional columnar crystals.

Consequently, cooling rate of 15 m s^{-1} would be the appropriate one for the new preparation method to obtain high performance Mg_2Ni alloy. After 10 cycles, the dramatic capacity decay for the MFRQ alloy is probably caused by the pulverization of the alloy due to the strong internal strain and the following serious corrosion.

3.4. Polarization analysis

The potentiodynamic polarization curves are presented in Fig. 9 to investigate the corrosion behaviors of the alloys (without pre-charge). The corrosion current density I_{corr} and the Tafel constants b_a , b_c are the fitted parameters derived from the Butler–Volmer equation in micro-region potentials [25]:

$$I = I_{\text{corr}} \left(e^{\frac{\eta}{b_a}} - e^{\frac{\eta}{b_c}} \right) \quad (2)$$

where I , η are experimentally obtained current and overpotential, respectively. Apparently, the corrosion potential E_{corr} of the MFRQ alloy shifts to the positive direction and the corrosion current density I_{corr} decreases, as compared to those of the as-cast alloy, implying an improved anti-corrosion property for the MFRQ alloy. Considering that the alloys have been passivated and the electrode surfaces have been considerably changed in the anodic polarization region, only the cathodic polarization curves are utilized to calculate

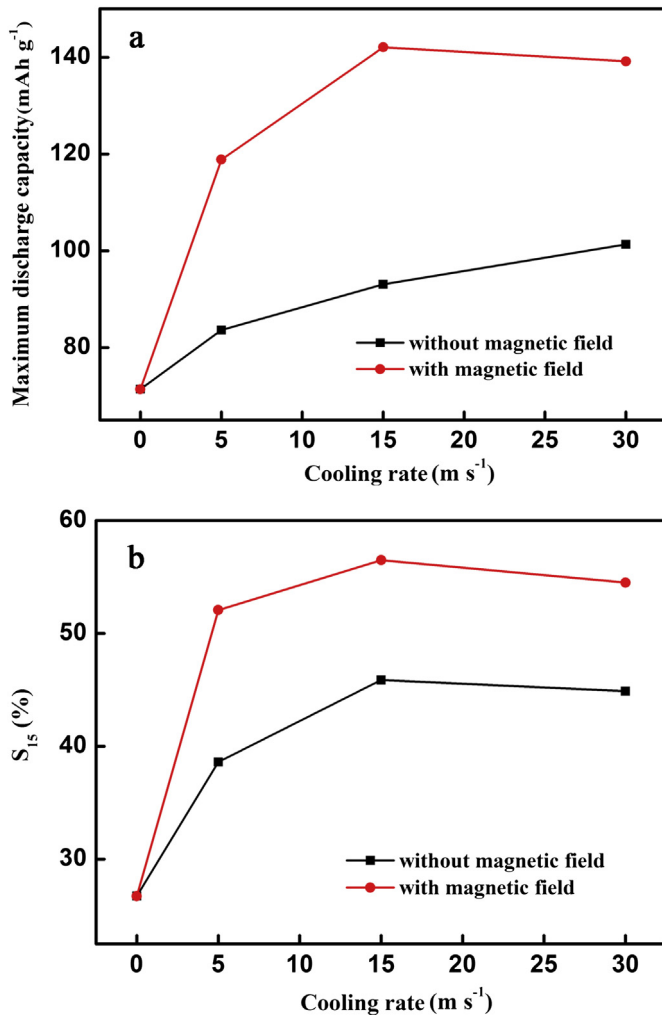


Fig. 8. Evolution of the maximum discharge capacities (a) and the cycle stabilities (b) of different alloys with the quenching rate.

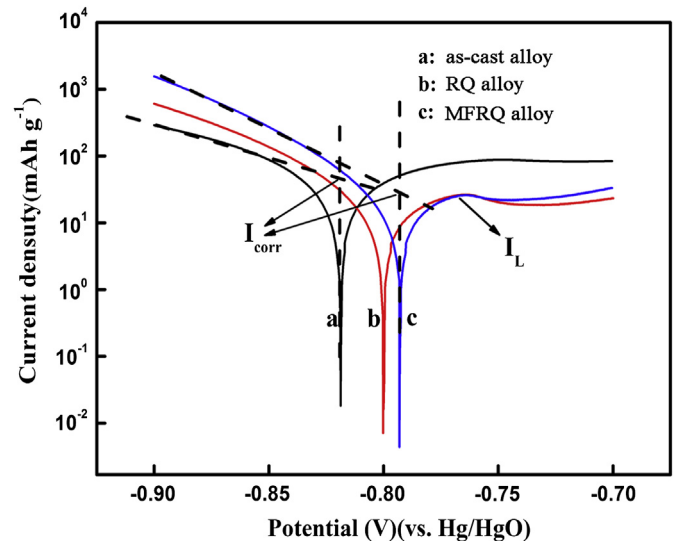


Fig. 9. Potentiodynamic polarization curves of the alloys.

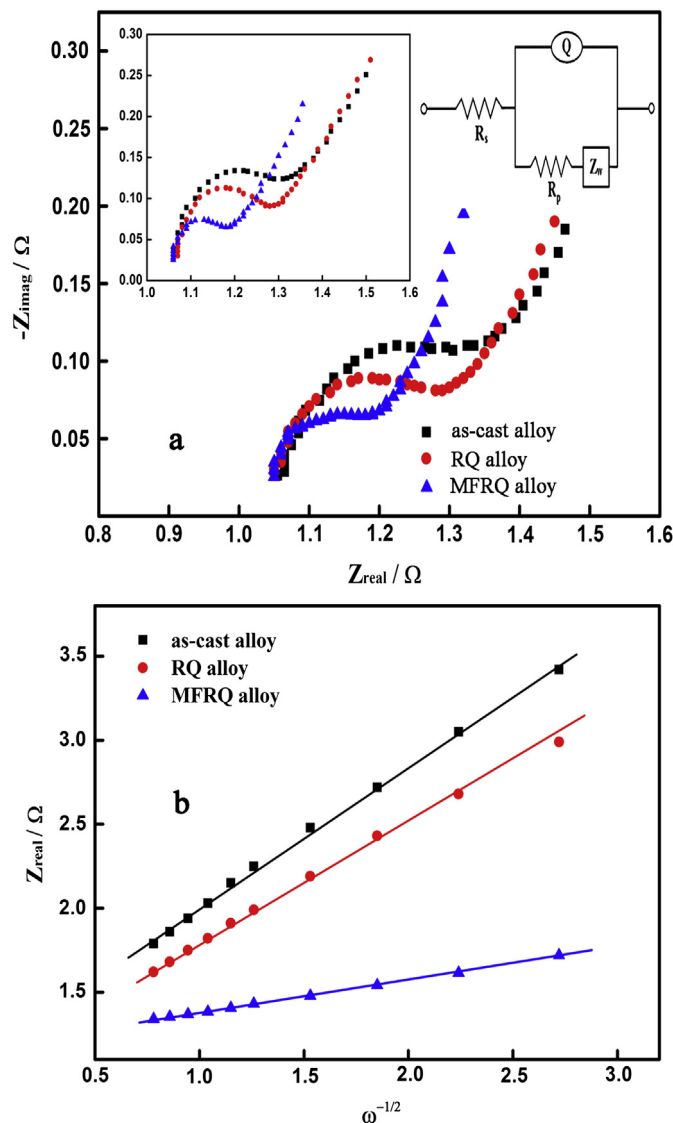


Fig. 10. EIS plots (a) and linear fitting of the Z_{real} vs. $\omega^{-1/2}$ relationships (b) for different alloys. The figure inset on the left-above is the fitting curves.

the I_{corr} . It is viewable that the anodic current densities of the RQ and MFRQ alloys first increase to a limiting value I_L and then decline, indicating that some hydrogen atoms are adsorbed on the electrode surfaces in the cathodic polarization region, and an oxidation reaction of the adsorbed hydrogen takes place in the anodic polarization region. In general, the anode process of the alloy electrode consists of an activation region and a passivation region, and the limiting current density I_L acts as an interface between these two regions. Besides this, the RQ and MFRQ alloys with high limiting current density have higher electrocatalytic activity compared to the as-cast alloy with feeble limiting current density [26].

3.5. Electrochemical impedance spectra analysis

EIS plots conducted in the frequency range from 10 kHz to 10 mHz with an AC amplitude of 5 mV are depicted in Fig. 10(a). Each Nyquist plot consists of a depressed capacitive semicircle at high frequency due to the charge-transfer process and a slope at low frequency, which is associated with the semi-infinite diffusion of H atoms into the bulk alloy. Herein, we used the equivalent

circuit model proposed by N. Cui et al. [27] to represent the EIS, in which the semicircle at high frequency region is due to the charge transfer resistance R_p , the straight line at low frequency is associated with the Warburg impedance Z_w , R_s is the ohmic resistance and Q is the double layer capacitance. Note that the equivalent circuit model fits the EIS spectra in our experiment very well. Thus, it is qualified to utilize such equivalent circuit to simulate the electrode process. It can be seen that the charge transfer resistance of the MFRQ alloy is greatly decreased in comparison with that of the as-cast alloy or the RQ alloy, which means an elevated electrochemical reaction rate and enhanced kinetic performance for the MFRQ alloy.

The hydrogen diffusion coefficient could be calculated by EIS using the following equation [28]:

$$D = \frac{0.5R^2T^2}{n^4F^4c^2\sigma^2} \quad (3)$$

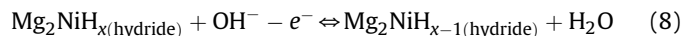
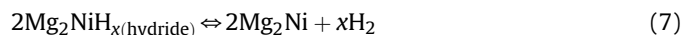
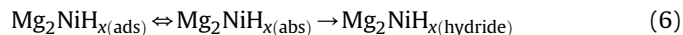
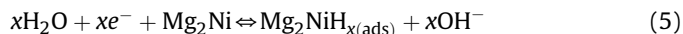
In this equation, R is the gas constant, T is the absolute temperature, n is the number of electrons per species reaction, F is the Faraday constant, c is the hydrogen concentration in the bulk of the alloy, and σ is the Warburg coefficient which obeys the following relationship:

$$Z_{\text{real}} = R_s + R_p + \sigma\omega^{-1/2} \quad (4)$$

Fig. 10(b) displays the linear fitting of Z_{real} vs. $\omega^{-1/2}$, from which the slope σ can be obtained. It can be seen from Equation (4) that there is no point in figuring out the exact value of D , as the effect of mass transfer can also be manifested through the Warburg coefficient σ . From Fig. 10(b), it is easy to deduce that the hydrogen diffusion of the quenching alloy in magnetic field is accelerated. Two reasons are mostly responsible for this result. Firstly, hydrogen diffusion is supposed to be enhanced due to grain boundary diffusion caused by the refinement of the grain [29]. Secondly, directional columnar structures supply channels for hydrogen diffusion.

3.6. Cyclic voltammetry analysis

The hydrogen evolution reaction at Mg_2Ni alloy electrode in an alkaline solution during charge and discharge can be represented as follows [30,31]:



where $\text{Mg}_2\text{NiH}_{\text{x(ads)}}$ and $\text{Mg}_2\text{NiH}_{\text{x(abs)}}$ are denoted as adsorbed hydrogen and absorbed hydrogen, $\text{Mg}_2\text{NiH}_{\text{x(hydride)}}$ refers to the hydrogen in the bulk of metal hydride. The electro-reduction of water with hydrogen adsorption (5) is followed by process of hydrogen diffusion into the bulk alloy and forming the hydride (6), which can be decomposed by either nonelectrochemical recombination (7) or electrochemical oxidation (8).

Based on the above analysis, cyclic voltammetry was performed at different scan rates to investigate the electrochemical hydrogen adsorption–oxidation behavior of the three alloys (Fig. 11). It is evident that no cathodic peak can be observed for the as-cast and RQ alloys when the scan rates are 1 and 10 mV s^{-1} . Whereas for the MFRQ alloy, the cathodic peak is around -0.85 V due to the reduction of H_2O with the adsorption of hydrogen on the alloy

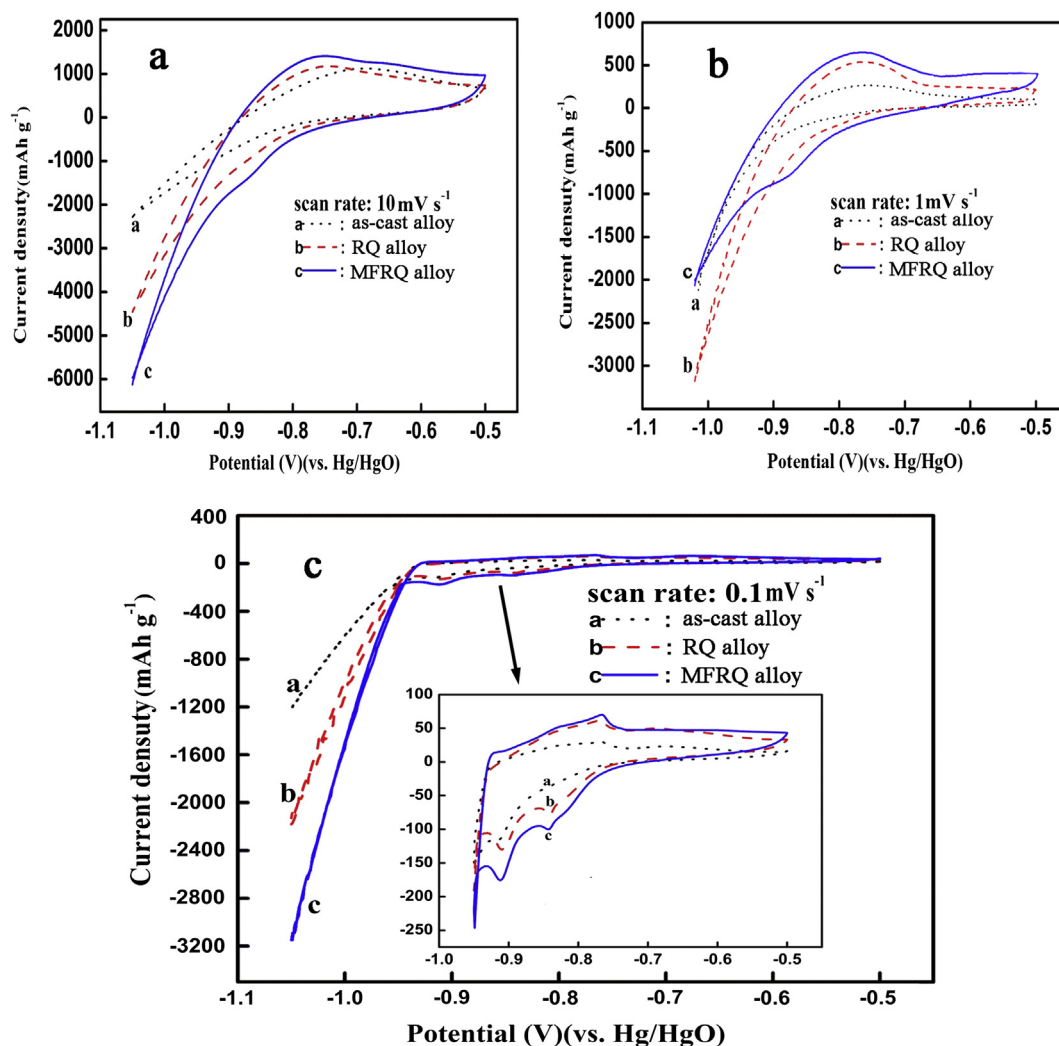


Fig. 11. CV curves of the three alloys at different scan rates: (a) 10 mV s^{-1} ; (b) 1 mV s^{-1} ; (c) 0.1 mV s^{-1} .

surface and the anodic peak is around -0.76 V owing to the oxidation of hydrogen. Additionally, the electrochemical oxidation and deoxidization peaks of hydride can also be observed at around -0.92 V when the scan rate is 0.1 mV s^{-1} . It is well known that reaction of high reversibility with diffusion being the rate determining step displays symmetric peak pairs, thus the fact at low scan rate (0.1 mV s^{-1}) suggests the presence of a quasi-reversible hydriding/dehydriding reaction. But in the case of high scan rates (1 and 10 mV s^{-1}), the reaction becomes completely irreversible. The change implies a transformation in the rate-determining step from hydrogen diffusion to charge transfer, i.e. the effect of mass transfer on the rate controlling is weakened with increasing scan rate. Generally, fast scan rate means serious polarization, which would lead to an irreversible electrode process. Nevertheless, the emergence of cathodic peak at high scan rate still reflects high reactive activity for the MFRQ alloy. This is consistent with the result of EIS. Moreover, compared with that of the as-cast and RQ alloys, the peak current and integrated peak area of the MFRQ alloy are much larger, implying a higher electrochemical capacity, which well agrees with the result of charge–discharge tests.

It is clear that the magnetic field leads to the formation of the directional columnar structures, which has profound effects on the electrochemical performance. In our opinion, the improved

electrochemical performance of the Mg_2Ni alloy treated by rapid quenching in magnetic field can be attributed to the following points: (1) the boundaries between the directional columnar structures not only provide huge numbers of fast diffusion channels for hydrogen diffusion, but also give gateways through which hydrogen could diffuse along, avoiding passing the closest packed crystal grains that can impede the diffusion; (2) transmission of energy into alloy from the magnetic field is probable during magnetic field treatment, and the introduction of this magnetic-field-induced defects (or called internal energy) would lower threshold for hydriding/dehydriding reaction and therefore give rise to an increasing reaction rate. Factually, the enhancement of electrochemical kinetics is found; (3) nickel-rich surfaces of the quenching alloys possess higher catalytic activity for hydrogen production, while the abundance of Mg in the as-cast alloy surface facilitates the irreversible oxidation of the alloy, leading to the formation of stable $\text{Mg}(\text{OH})_2$ film, which will block the paths for hydrogen diffusion. It is worth emphasizing that the negative influence caused by the magnetic-field-induced internal strain on the cycle stability is far insufficient in comparison with that positive effect due to the structure of directional columnar crystals, as the MFRQ alloy with high internal strain displays better cycling performance compared to the RQ alloy with low internal strain.

4. Conclusions

The investigation of the microstructures revealed that Mg₂Ni showed a remarkable magnetic anisotropy. The alloy after being rapidly quenched in magnetic field had directional columnar structures with fine grain size, homogeneous composition and high internal strain. However, the growth of crystals in magnetic field tended to be more random with increasing quenching rate. The electrochemical discharge capacity was increased and the cycle stability was improved after the Mg₂Ni alloy was rapidly quenched in magnetic field. The MFRQ alloy with quenching rate of 15 m s⁻¹ exhibited improved electrochemical properties with a discharge capacity of 142.05 mAh g⁻¹ and capacity retention ratio of 56.5% after 15 cycles. In addition, enhancement of electrochemical kinetics was also found for the MFRQ alloy from the results of EIS and CV. Herein, we provide a very promising strategy, quenching in the magnetic field for modification of Mg₂Ni alloy.

Acknowledgments

The authors greatly appreciate the financial support from the National Nature Science Foundation of China (No. 20971129), Chongqing Natural Science Foundation (cstc2011jjA0780), Scientific Research Foundation of Central South University and Post-doctoral Science Fund Program of Central South University.

References

- [1] Y.F. Liu, H.G. Pan, M.X. Gao, Q.D. Wang, *J. Mater. Chem.* 21 (2011) 4743–4755.
- [2] B. Sakintuna, F. Lamari-Darkrim, M. Hirscher, *Int. J. Hydrogen Energy* 32 (2007) 1121–1140.
- [3] T. Kohno, S. Tsuruta, M. Kanda, *J. Electrochem. Soc.* 143 (1996) L198–L199.
- [4] S. Nohara, N. Fujita, S.G. Zhang, H. Inoue, C. Iwakura, *J. Alloys Compd.* 267 (1998) 76–78.
- [5] M.Y. Song, S.N. Kwon, J.S. Bae, S.H. Hong, *Int. J. Hydrogen Energy* 33 (2008) 1711–1718.
- [6] S.K. Zhang, K.Y. Shua, Y.Q. Lei, G.L. Lu, Q.D. Wang, *Int. J. Hydrogen Energy* 28 (2003) 977–981.
- [7] K.Y. Shu, X.G. Yang, S.K. Zhang, G.L. Lu, Y.Q. Lei, Q.D. Wang, *J. Power Sources* 96 (2001) 288–292.
- [8] Y.H. Zhang, M.Y. Chen, X.L. Wang, G.Q. Wang, Y.F. Lin, Y. Qi, *J. Power Sources* 125 (2003) 273–279.
- [9] F.S. Wei, Y.Q. Lei, L.X. Chen, G.L. Lu, Q.D. Wang, *Int. J. Hydrogen Energy* 32 (2007) 2935–2942.
- [10] L.J. Huang, J.G. Tang, G.Y. Liang, Y. Wang, D.C. Wu, *J. Power Sources* 189 (2008) 1247–1250.
- [11] G.Y. Liang, D.C. Wu, L. Li, L.J. Huang, *J. Power Sources* 186 (2009) 528–531.
- [12] Y.H. Zhang, B.W. Li, Z.H. Ma, S.H. Guo, Y. Qi, X.L. Wang, *Int. J. Hydrogen Energy* 35 (2010) 11966–11974.
- [13] L.Z. Ouyang, H. Wang, M. Zhu, J. Zou, C.Y. Chung, *J. Alloys Compd.* 404–406 (2005) 485–489.
- [14] X. Li, Y. Fautrelle, Z.M. Ren, *Acta Mater.* 55 (2007) 1377–1386.
- [15] Y.B. Zuo, J.Z. Cui, Z.H. Zhao, *J. Mater. Sci.* 47 (2012) 5501–5508.
- [16] T. Zhang, W.L. Ren, J.W. Dong, X. Li, Z.M. Ren, G.H. Cao, Y.B. Zhong, *J. Alloys Compd.* 487 (2009) 612–617.
- [17] P. Lehmann, R. Moreau, D. Camel, R. Bolcato, *Acta Mater.* 46 (1998) 4067–4079.
- [18] R. Kainuma, Y. Imano, W. Ito, Y. Sutou, H. Morito, S. Okamoto, O. Kitakami, K. Oikawa, A. Fujita, T. Kanomata, K. Ishida, *Nature* 439 (2006) 957–960.
- [19] B. Ganapathysubramanian, N. Zabaras, *J. Cryst. Growth* 270 (2004) 255–272.
- [20] X. Li, Y. Fautrelle, Z.M. Ren, *J. Cryst. Growth* 306 (2007) 187–194.
- [21] R.C. O'Handley, *J. Appl. Phys.* 83 (1997) 3263–3270.
- [22] S.N. Danilchenko, O.G. Kukharensko, C. Moseke, I.Y. Protsenko, L.F. Sukhodub, B. Sulkio-Cleff, *Cryst. Res. Technol.* 37 (2002) 1234–1240.
- [23] V. Uvarov, I. Popov, *Mater. Charact.* 58 (2007) 883–891.
- [24] P.A. Algarabel, C. Magen, L. Morellon, M.R. Ibarra, F. Albertini, N. Magnani, A. Paoluzi, L. Pareti, M. Pasqualetto, S. Besseghini, *J. Magn. Magn. Mater.* 272–276 (2004) 2047–2048.
- [25] C.N. Cao, *The Principles of Corrosion Electrochemistry*, Chemical Industry Press, Beijing, 2004.
- [26] X.P. Dong, Y.H. Zhang, F.X. Lu, L.Y. Yang, X.L. Wang, *Int. J. Hydrogen Energy* 32 (2007) 4949–4956.
- [27] N. Cui, B. Luan, H.K. Liu, S.X. Dou, *J. Power Sources* 63 (1996) 209–214.
- [28] X.X. Yuan, N.X. Xu, *J. Alloys Compd.* 329 (2001) 115–120.
- [29] A.M. Brass, A. Chanfreau, *Acta Mater.* 44 (1996) 3823–3831.
- [30] N. Cui, J.L. Luo, K.T. Chuang, *J. Electroanal. Chem.* 503 (2001) 92–98.
- [31] H. Niu, D.O. Northwood, *Int. J. Hydrogen Energy* 27 (2002) 69–77.